

## EVIDENCE OF RAPID FLUX EMERGENCE ASSOCIATED WITH THE M8.7 FLARE ON 2002 JULY 26

HAIMIN WANG,<sup>1,2</sup> JIONG QIU,<sup>2</sup> JU JING,<sup>1,2</sup> THOMAS J. SPIROCK,<sup>1,2</sup> VASYL YURCHYSHYN,<sup>1</sup>  
VALENTINA ABRAMENKO,<sup>1</sup> HAISHENG JI,<sup>1</sup> AND PHILLIP R. GOODE<sup>1,2</sup>  
*Received 2003 October 31; accepted 2004 January 6*

### ABSTRACT

In this paper, we present a detailed study of the M8.7 flare that occurred on 2002 July 26 using data from the Big Bear Solar Observatory (BBSO), *Ramaty High Energy Solar Spectroscopic Imager (RHESSI)*, the *Transition Region and Coronal Explorer (TRACE)*, and the *Solar and Heliospheric Observatory (SOHO)*. This flare has interesting properties similar to a number of flares that we studied previously, such as a rapid increase of magnetic flux in one polarity and an increase in transverse fields and magnetic shear associated with the flare. However, this event had the most comprehensive observations; in particular, the high-resolution high-cadence BBSO vector magnetograph observations. At the time of the flare, across the flare neutral line, there was a sudden emergence of magnetic flux at the rate of  $10^{20}$  Mx hr<sup>-1</sup> in both the longitudinal and transverse components. The emerging flux mostly occurred at the sites of the flare. It was very inclined and led to impulsively enhanced shear in the magnetic fields. We discuss these observations in the context of magnetic reconnection triggered by rapid flux emergence. It is also possible that the new flux signifies flare-related change in the field line inclination.

*Subject headings:* Sun: activity — Sun: flares — Sun: magnetic fields

### 1. INTRODUCTION

Ever since the discovery of coronal mass ejections (CMEs), various CME models have been developed (see Forbes 2001 for a review). These include the flux rope model (Low 1994; Forbes & Priest 1995; Amari et al. 2000; Chen 1989), the sheared arcade reconnection model (e.g., Mikic & Linker 1994; Magara, Shibata, & Yokoyama 1997; Choe & Cheng 2002), and the breakout model (e.g., Antiochos, DeVore, & Klimchuk 1999). Regardless of different configurations depicted by different models, it is believed that the evolution of the magnetic fields at or below the photosphere, in the form of shear motion or flux emergence, results in the loss of equilibrium of the magnetic structure leading to the CME.

These changes of the photospheric magnetic fields should be studied observationally with respect to flares and CMEs. In terms of the magnetic flux change related to flares, several recent papers have provided some interesting observations. Kosovichev & Zharkova (2001) studied high-resolution Michelson Doppler Imager (MDI) magnetogram data for the 2000 July 14 “Bastille Day flare” and found permanent decreases in magnetic fluxes. It was explained by the release of magnetic energy. Spirock, Yurchyshyn, & Wang (2002) studied the X20 flare on 2001 April 2, one of the largest solar flares in the last few decades, and found that after the flare, the magnetic flux of the leading polarity increased by approximately  $6 \times 10^{20}$  Mx, while there was no obvious change in the magnetic flux in the following polarity. Wang et al. (2002a) summarized the study of six X-class flares and found that unbalanced and rapid flux increase might be a common property of major solar flares. Such an increased flux level lasted through the end of observations. It now becomes clear that with high-cadence (1 minute) and high-resolution (1''–2'') magnetic field observations, sudden flux changes associated with flares are observed to exist for at least some bigger

events. Note that all of the six events studied by Wang et al. (2002a) have flare-associated CMEs; therefore, studying flare-related magnetic field change will also shed light on the magnetic mechanism of CMEs. Green et al. (2003) carried out a systematic analysis of changes in the magnetic flux and polarity imbalance of four CME-productive solar active regions during their entire disk passage. They found that magnetic changes do not systematically accompany flares and CMEs, but when they do they are not permanent, having a typical lifetime of 6 hr. They also found short-term changes in the flux and a polarity imbalance of active regions that were not related to any major (M or X class) flare. Green et al. (2003) used 96 minute MDI data; in this study we use both BBSO and MDI data with 1 minute cadence.

In terms of the relationship between flares and the magnetic nonpotentiality, it has been established, from the early studies of the relationship of solar flares to the morphology of an active region’s magnetic field, that strong flares mostly occur near the neutral lines of the active region’s vertical component of the magnetic field where there is a strong gradient in the magnetic field and where the horizontal component is strongly sheared. This shear in the horizontal component may experience substantial flare-related changes. Wang et al. (1994) determined that the magnetic shear of an active region may increase after the occurrence of an X-class flare. This result initially appears to be counterintuitive, as the magnetic shear is expected to decrease as the total magnetic energy of the active region decreases. Chen et al. (1994) studied more than 20 M class flares and determined that there was essentially no apparent change in magnetic fields associated with the flares. The results from studies conducted at the Marshall Space Flight Center (Ambastha, Hagyard, & West 1993; Hagyard, Start, & Venkatakrishnan 1999) were inconclusive. The morphology of an active region’s magnetic field may or may not change, as the result of a solar flare and the magnetic shear in the active region may decrease, increase, or remain unchanged. Recent studies of Wang et al. (2002a) also point to an increased shear for two events. However, the conclusions of these attempts have not been unambiguous because it is not

<sup>1</sup> Big Bear Solar Observatory, New Jersey Institute of Technology, 40386 North Shore Lane, Big Bear City, CA 92314-9672; haimin@flare.njit.edu.

<sup>2</sup> Center for Solar and Terrestrial Research, New Jersey Institute of Technology, Newark, NJ 07102.

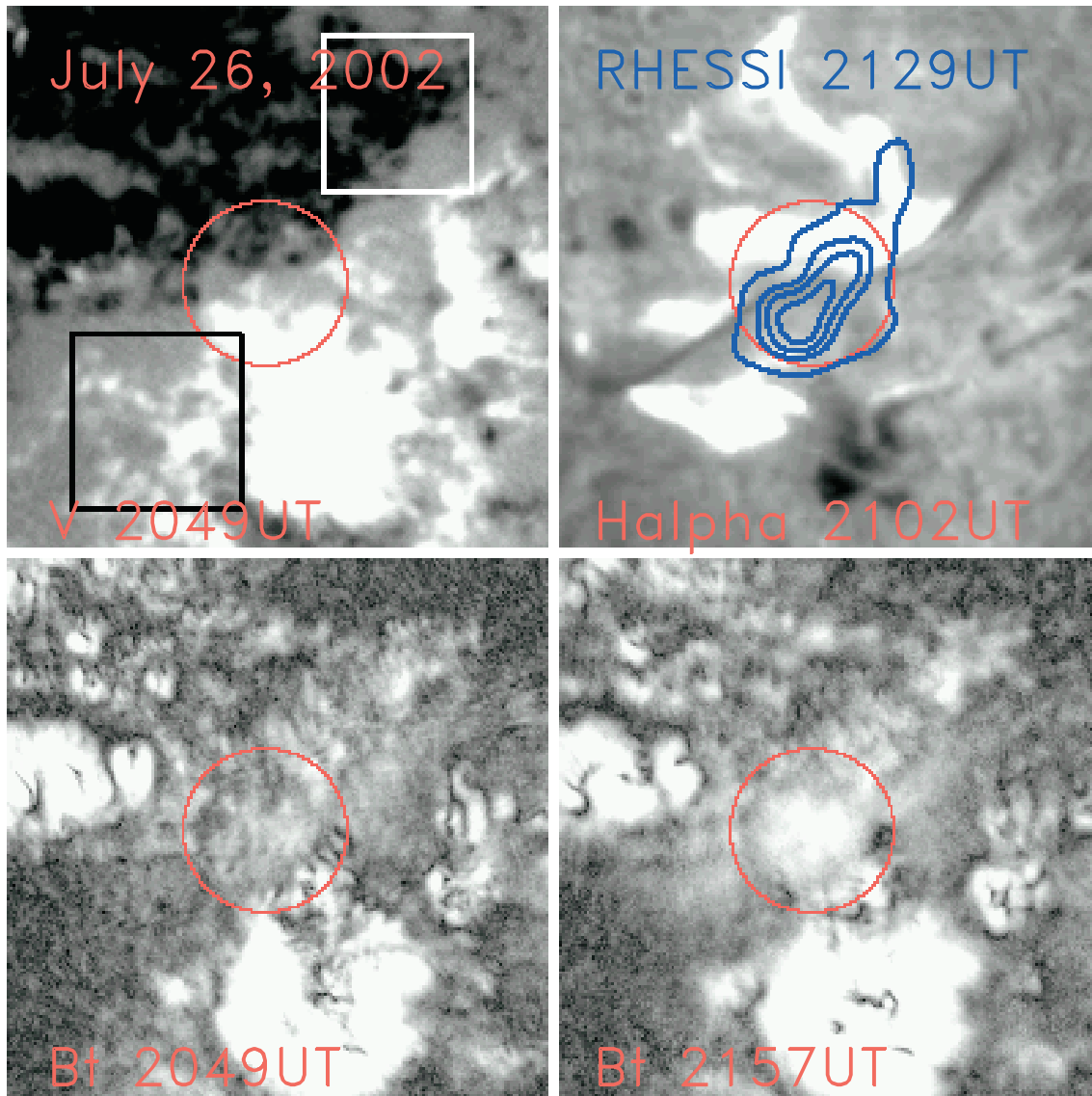


FIG. 1.—*Top left:* Line-of-sight magnetogram. *Top right:*  $H\alpha$  flare ribbons and *RHESSI* hard X-ray image (5–10 keV) after the peak of the flare. *Bottom:* Comparison of transverse magnetic field before and after the flare. Squares and circle are areas of enhancement of longitudinal and transverse magnetic fields. The field of view is  $120'' \times 120''$ .

easy to separate the tangential component contribution from other contributions, such as seeing and the decreased signal-to-noise ratio.

The event studied in this paper provides a very good opportunity to investigate the three-dimensional structure of the magnetic structure associated with the flare: the event was close to disk center, the seeing was very good and stable, and we had comprehensive coverage with BBSO vector magnetograph, *RHESSI*, and *TRACE* observations.

## 2. OBSERVATIONS AND DATA REDUCTION

BBSO's Digital Vector Magnetograph (DVMG) system has a much improved sensitivity and resolution compared to that of the old BBSO videomagnetograph system. The hardware has been described in detail by Spirock et al. (2002). It consists of a  $1/4 \text{ \AA}$  bandpass filter, an SMD  $1024 \times 1024$  12 bit CCD camera, and three liquid crystals used as polarization analyzers. Each data set consists of four images: a  $6103 \text{ \AA}$  filtergram (Stokes  $I$ ), a line-of-sight magnetogram (Stokes  $V$ ), and the transverse magnetogram (Stokes  $U$  and  $Q$ ). We usually

rebin the camera to the  $512 \times 512$  mode to increase the sensitivity of the magnetograms. After rebinning, the pixel resolution is about  $0''.6$ . The line-of-sight magnetic sensitivity is approximately 2 G, while the transverse sensitivity is approximately 20 G. The cadence for a complete set of Stokes images is typically 1 minute.

BBSO magnetograms cover a time range from 19 to 00 UT. In order to cover a longer time period and also have an independent confirmation of BBSO observations, we used high-resolution, high-cadence line-of-sight magnetograms from *SOHO* MDI. MDI mainly obtains full-disk Dopplergrams for the investigation of solar oscillations. In addition, MDI provides full-disk longitudinal magnetograms with a cadence of 1 minute and an image scale of  $2''$  for some observing days (Scherrer et al. 1995).

In the past two and a half years, we have successfully installed and are continuously operating a high-resolution global  $H\alpha$  network. The stations are at BBSO, the Kanzelhöhe Solar Observatory (KSO) in Austria, the Catania Astrophysical Observatory (CAO) in Italy, the Yunnan Observatory (YO),

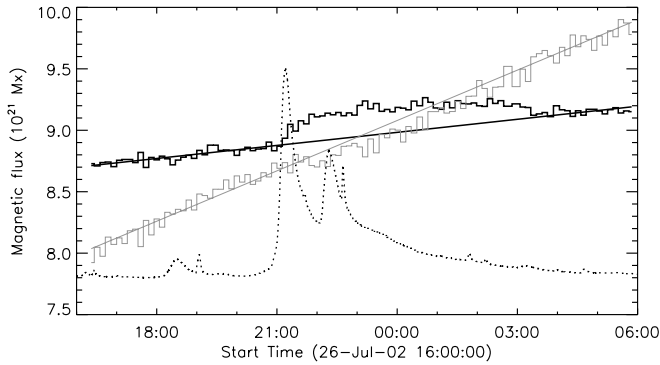


FIG. 2.—Evolution of magnetic flux over the entire field of view of Fig. 1. The measurements are from MDI magnetograms. The darker solid lines are for positive flux and its linear fit; the lighter solid lines are for negative flux; the dotted line shows *GOES* soft X-ray flux. In addition to the flare presented in this study, there were two other flares (M5.3 peaked at 2217 UT, and M4.6 peaked at 2238 UT) in the same active region. However, they were associated with different magnetic neutral lines.

and the Huairou Solar Observing Station (HSOS) in China. Nominally, each station obtains  $H\alpha$  images every minute with  $1''$  pixel resolution. The data are calibrated using standard procedures from BBSO. The primary data to locate flare sources in the current study are from full-disk  $H\alpha$  data obtained at BBSO.

This event was covered by *TRACE*. It is a powerful instrument linking dynamic phenomena from the chromosphere through the transition region to the corona (Handy et al. 1999). *TRACE* usually covers a field ( $510'' \times 510''$ ) that is larger than, but comparable to, the field of view of BBSO high-resolution observations ( $300'' \times 300''$ ). For the event studied, *TRACE* covered different wavelengths before and after the flare ( $1600 \text{ \AA}$  before and  $171 \text{ \AA}$  after), as the flare triggered the corona observing mode. We concentrate our study on the postflare loop structure.

Much of the energy released during a flare is used to accelerate electrons (primarily emitting X-rays) to very high energies and protons and other ions (primarily emitting gamma rays). The new approach of *RHESSI* is to combine, for the first time, high-resolution imaging in hard X-rays and gamma rays with high-resolution spectroscopy, so that a detailed energy spectrum can be obtained at each point of the image (Lin et al. 2002). Such information advances our understanding of the fundamental high-energy processes at the core of the solar flare problem. *RHESSI* had postpeak coverage on this flare. We were able to make maps from the available data.

According to the CME list compiled by the Large Angle and Spectrometric Coronagraph Experiment (*LASCO*) team, this event was accompanied by a fast halo CME that began to be observed by C2 at 22:30 UT, and its average speed was  $800 \text{ km s}^{-1}$ .

### 3. RESULTS

#### 3.1. Measurements of Vector Magnetic Fields

As in our earlier studies, we first search for changes in the magnetic fields, which include line-of-sight magnetic fields (from measurement of circular polarization  $V$ ) and transverse magnetic fields (from measurements of linear polarization  $Q$  and  $U$ ). The amplitude of the transverse field is determined by

$$B_T = C(Q^2 + U^2)^{1/4},$$

where  $C$  is a calibration constant, and the azimuthal angle is determined by

$$\theta = \frac{1}{2} \arctan\left(\frac{U}{Q}\right).$$

In a previous paper (Wang 1992), we defined the term “shear” as the product of the shear angle and the measured transverse field strength. This term was introduced to describe the magnetic shear in solar active regions. The shear angle is the angular difference between the transverse component of the model potential field and the measured transverse field. We introduced this definition of shear, instead of the pure shear angle defined by Hagyard et al. (1984) and Hagyard, Venkatakrishnan, & Smith (1990) because (1) the strong transverse field regions contribute more significantly to the free magnetic energy of shear, and (2) the measurement errors in the azimuthal angles for strong field regions are significantly reduced. Since every point has a well-defined magnetic shear, two-dimensional shear maps can be constructed. The

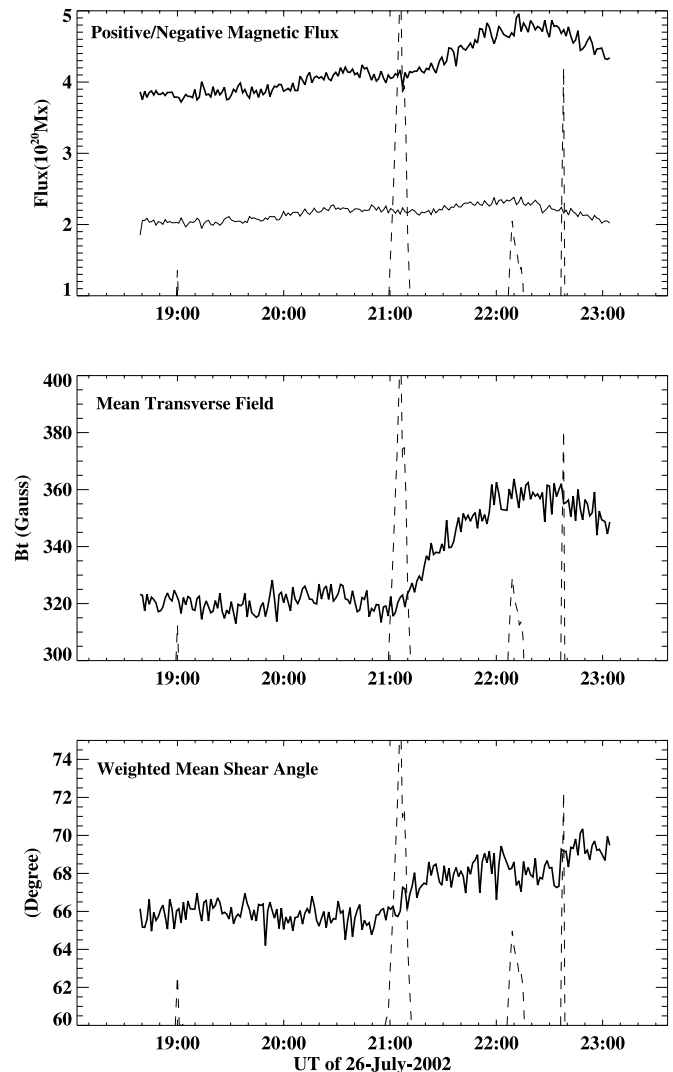


FIG. 3.—Time profiles of line-of-sight magnetic field, transverse field, and weighted mean shear angle from BBSO data. The dashed lines are derivatives of *GOES* X-ray flux. *Top*: Thicker line is positive magnetic flux, and lighter line is negative magnetic flux. The transverse fields are measured within the red circle in Fig. 1, while positive fluxes are inside the black box and negative fluxes are inside the white box.

time sequence of shear maps is compiled as shear movies in order to visualize evolution of the magnetic shear.

### 3.2. Flare-Related Changes of Magnetic Fields

To demonstrate the morphology of the flare and relative position in the magnetograms, Figure 1 shows a BBSO line-of-sight magnetogram shortly before the flare, an  $H\alpha$  image overplotted by *RHESSI* contour in the energy range of 5–10 keV right after the flare peak, and a comparison of transverse magnetic fields before and after the flare. The red circle marks the area of a rapid increase of the transverse magnetic field, which is cospatial with the *RHESSI* loop-top source and connects two  $H\alpha$  ribbons.

Figure 2 plots the positive and negative line-of-sight magnetic flux, in absolute values, in the entire field of view ( $120'' \times 120''$ ) shown in Figure 1. The magnetograph data were from MDI, which covered a much longer period and are free of atmospheric seeing. The *GOES* X-ray light curve is overplotted to show the evolution of the flare emission. The figure shows that there is a continuous increase in both the positive and negative flux over 14 hr, which is caused mainly by gradual new flux emergence that moved to the field of view. This trend can be approximated by a linear function of time, as shown in Figure 2. Apart from this linear evolution, we also find a rapid increase of the magnetic flux in the positive polarity at the time of the M8.7 flare. With the linear trend subtracted, the rapid rise of the positive flux amounts to  $2 \times 10^{20}$  Mx. The negative magnetic fields do not exhibit significant change relative to the linear trend. The bump in Figure 2 lasts about 6 hr, in agreement with the timescale of magnetic flux changes presented by Green et al. (2003). After 6 hr, the emerged flux did not disappear; the growth rate simply dropped. The flare-related magnetic flux change motivated us to study the higher resolution BBSO vector magnetograms in more detail to pin down the location and the nature of such a rapid change.

Figure 3 plots the temporal evolution of the line-of-sight magnetic flux, mean transverse field strength, and magnetic

shear, using the vector magnetic field observations by BBSO during 19–23 UT. The coordinates of the center of the field of view is  $306''$  east and  $78''$  north. Here we summarize the major results.

1. The positive magnetic flux evolves in the same pattern as shown in the MDI magnetograms. We can pinpoint the area that contributed to the increase of the positive flux: at one of the flare footpoints marked by the black box. Figure 3 shows that the positive flux integrated over the black box rapidly increased by  $1.3 \times 10^{20}$  Mx over about 1 hr, which confirms that most of the positive flux increase occurs at the site of the flare. The positive flux change rate is about  $1 \times 10^{20}$  Mx  $\text{hr}^{-1}$  at the maximum. The BBSO magnetograms also show slight negative flux increase in the white box. The observed trend of the negative flux is somehow different from MDI observations, because some long-term changes in MDI data are due to motions of fluxes in and out the field of view.

2. The mean transverse field strength increased rapidly by 40 G, or about 6% of the preflare fields, within an hour after the onset of the flare, and the area of the most obvious increase is between two footpoints, as marked by the circle in Figure 1. Assuming that the emerging flux loop has a diameter of  $\sim 20''$ , the transverse flux increases by about  $6.5 \times 10^{20}$  Mx at the maximum, and the peak flux rising rate is larger than the longitudinal flux increase rate. This indicates an inclined (flat) flux emergence.

3. The figure shows that the area before the flare have a moderate weighed mean magnetic shear of  $66^\circ$ . Throughout the flare, the shear increases by  $4^\circ$  following the same pattern as the transverse field strength. The increase in the magnetic shear indicates that the magnetic fields become less potential after the flare.

4. No change was found for the mean brightness (not shown in the figure); there is no evidence of sunspot appearance or disappearance (e.g., Wang et al. 2002b) associated with the flare. This also indicates that the changes in the magnetic field are not due to change of line profile in the observation. Such a conclusion is further supported by the analysis of line profile

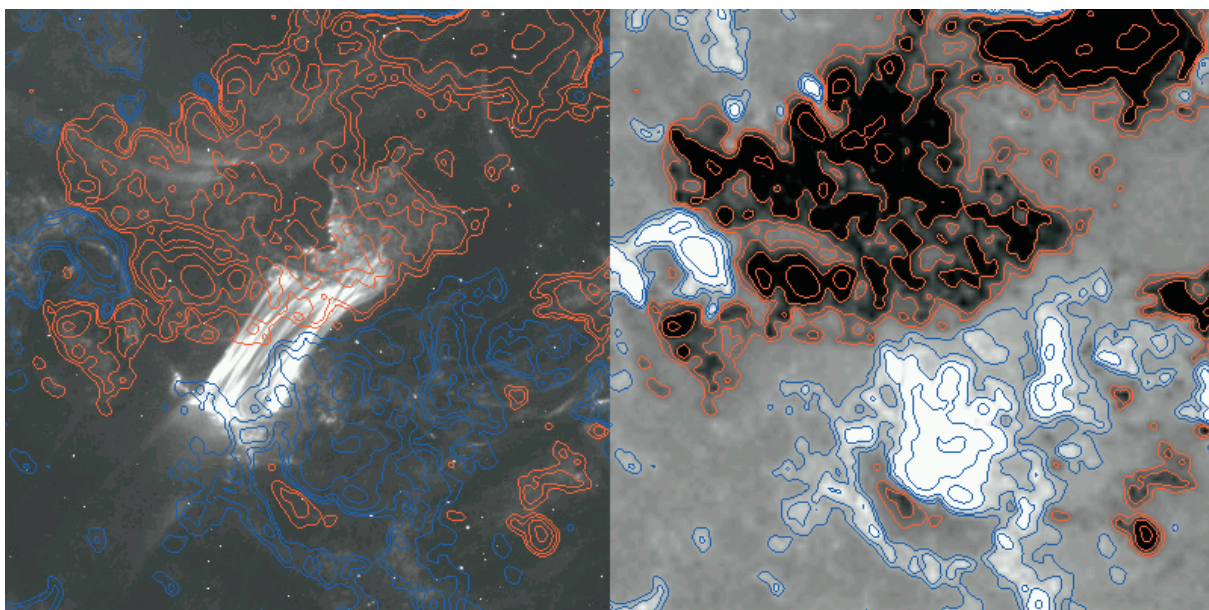


FIG. 4.—*Left*: Comparison of contours of a magnetogram with *TRACE* 171 Å image after the peak of the flare. *Right*: Comparison of the gray-scale magnetogram with its contours. The field of view is  $200'' \times 200''$ .

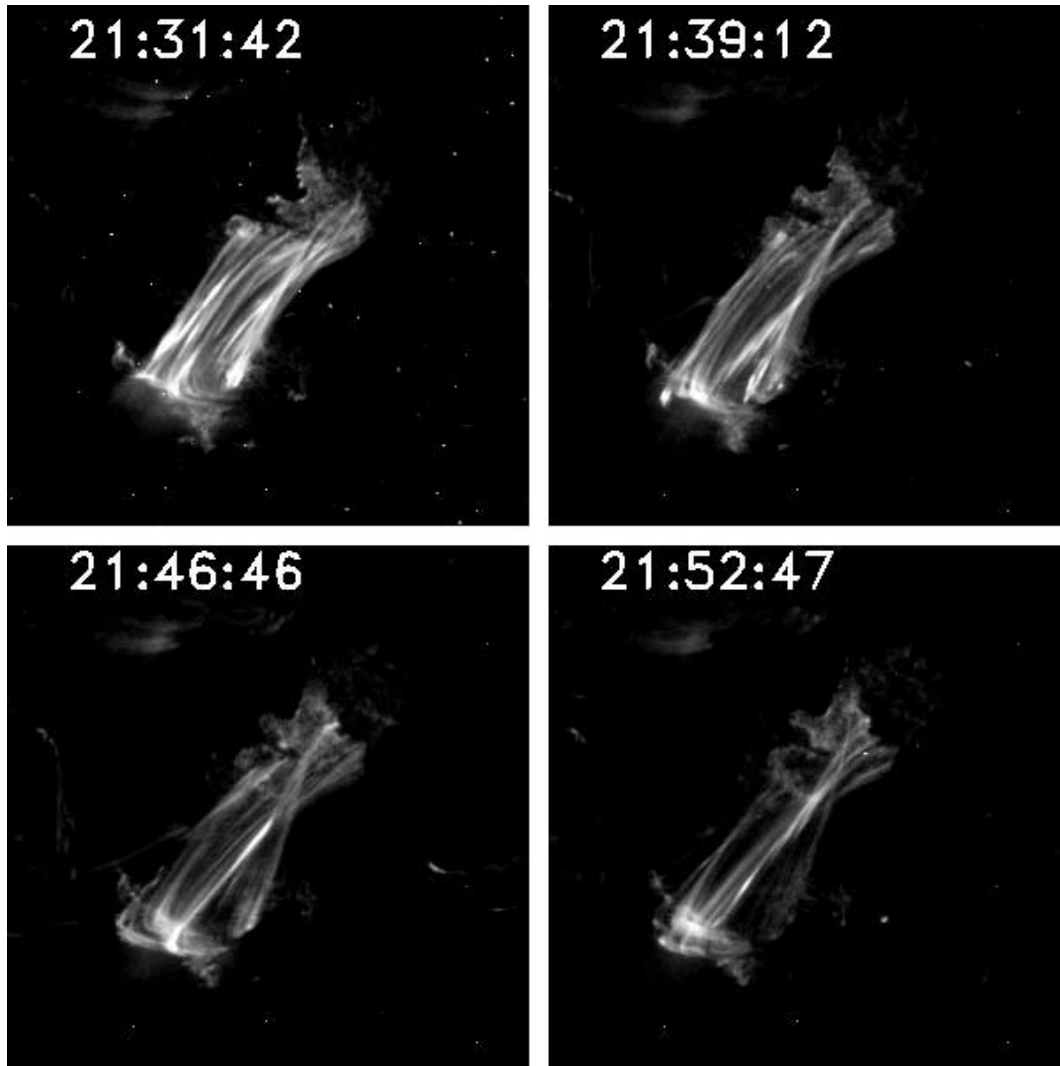


FIG. 5.—Sequence of *TRACE* images showing the slowly rising post-flare loop. The field of view is  $200'' \times 200''$ .

associated with this flare using the Imaging Vector Magnetograph at Haleakala, the University of Hawaii (Ji et al. 2004).

These observations indicate rapid increase of both the magnetic flux and magnetic nonpotentiality at the site of the flare, and the rate of the flare-related flux change is of order  $10^{20} \text{ Mx hr}^{-1}$  in both the longitudinal and transverse flux. These further suggest that a significant amount of sheared and inclined magnetic flux is impulsively injected into the site of the flare. We used 4 hr time sequence of BBSO data (2 hr before and 2 hr after the event). The MDI data in Figure 2 covers 5 hr before and 9 hr after the flare.

### 3.3. Evolution of Flare and Filament

The  $\text{H}\alpha$  observations show two bright flare ribbons residing in magnetic fields of opposite polarities, as shown in Figure 1. These two ribbons are connected by the hard X-ray source seen by *RHESSI*.  $\text{H}\alpha$  observations reveal that both ribbons exhibit expansion motion away from the magnetic neutral line during the impulsive phase. The expansion velocity profiles of the two ribbons are temporally correlated, both reaching the maximum at 21:05 UT, around the maximum of the flare. *TRACE* observed the flare in the coronal line during the decay phase. Figure 4 compares the *TRACE* 171 Å image with a

corresponding magnetogram. The two  $\text{H}\alpha$  ribbons are clearly linked by the *TRACE* loops. Figure 5 shows the evolution of the *TRACE* 171 Å loops that keep rising over several hours after the flare maximum. In addition, the alignment of these post-flare loops is not nearly vertical to but much inclined to the magnetic neutral line, suggesting sheared magnetic loops.

Observations of the expanding ribbons in  $\text{H}\alpha$  and rising post-flare EUV loops that connect the two ribbons suggest continuous formation of flare loops at rising altitudes, as would be described by the standard flare model (see Forbes & Acton 1996 and references therein). In a macroscopic description, the rate of the magnetic reconnection, in terms of the electric field  $E_{\text{rec}}$  at the coronal reconnection site, can be inferred from the expansion velocity of the flare ribbons and the magnetic field strength swept by the ribbons (Forbes & Priest 1984; Forbes & Lin 2000; Qiu et al. 2002). Figure 6 shows the velocity profiles of the ribbon expansion and the inferred reconnection electric field from the two ribbons, respectively. As we did not have complete hard X-ray light curves, we use the derivative of *GOES* soft X-ray flux to represent hard X-ray flux, which is overplotted in the figure. The derived  $E_{\text{rec}}$ , taken as an average of the measurements from the two ribbons, is of order  $3 \text{ V cm}^{-1}$  at the flare

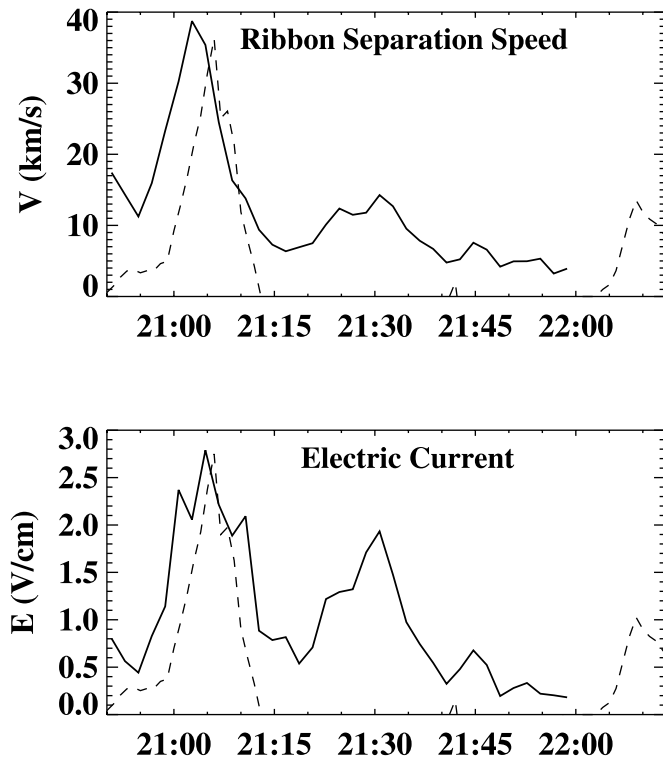


FIG. 6.—*Top*: Mean flare ribbon separation speed as a function of time overplotted by the derivative of *GOES* X-ray flux (*dashed line*). *Bottom*: Derived electric field in the reconnection region as a function of time.

maximum, which is comparable with the value of  $6 \text{ V cm}^{-1}$  derived by Qiu et al. (2004) for an X1.6 flare.

On the other hand, we also find that this flare is different from other events, such as those studied by Wang et al. (2002a) and Qiu et al. (2004). This flare is not preceded by filament eruption. Although there is a filament right in the middle of the two ribbons, it remains still throughout the flare. Apparently, the rising post-flare loops are formed above the filament so that the filament is not disturbed at all by the flare or CME. These observations suggest that this event does not comply with the flux rope model in a bipolar inverse configuration, in which case the reconnection and formation of coronal loops would take place below the filament (e.g., Low & Zhang 2002).

#### 4. DISCUSSION

This event provided a remarkably clear example of rapid flux emergence, which shows an increase in the transverse fields in the middle of the loop and an increase in the longitudinal fields near the footpoints. The increase of the magnetic flux amounts to several times  $10^{20} \text{ Mx}$  in both the longitudinal and transverse components in a timescale of several tens of minutes. Therefore, the peak flux change rate is of order  $10^{20} \text{ Mx hr}^{-1}$ . Such changes are accompanied by the enhancement of magnetic nonpotentiality, as represented by the increase of the magnetic shear after the flare. We also note that

although the flare is accompanied by a halo CME, the surface magnetic field changes took place mostly at the sites of the flares. This may suggest that the trigger of the mass ejection is rather localized. Any model that can be used to interpret this observation needs to take into consideration the following points.

1. A rapid increase of transverse fields following the flare shows a rising, very inclined loop going through the photosphere. The increased magnetic shear is an indicator that the emerged loop is very much sheared.

2. The field lines are very inclined, as the *TRACE* post flare loops are very flat. This is also supported by the unbalanced flux increase. As we discussed in previous papers (e.g., Wang et al. 2002a), if the region is  $\theta$  away from the disk center, newly emerged flux will appear in one polarity—the polarity closer to the limb, provided that the inclination angle of the field line of the new flux is  $\theta$  or smaller. For this event  $\theta = 20^\circ$ , so the inclination angle is about  $20^\circ$ , consistent with the appearance of *TRACE* loop. This is also in agreement with the results of Green et al. (2003).

3. This rising loop is part of (or a triggering of) a large loop system in the corona, which lost equilibrium and expanded to form the flare and CME. Based on *LASCO* observations, this CME does not have the classic three components: front, cavity, and filament. The filament in  $\text{H}\alpha$  in the neutral line did not erupt. Therefore, there is no evidence of opening of field lines by the eruption.

4. The flare itself shows some properties of a typical two-ribbon flare. Most notable is the separation of the two  $\text{H}\alpha$  ribbons. As we show in Figure 6, the strongest E field coincides with the peak of the hard X-ray, agreeing with the conclusion of Qiu et al. (2004). This indicates a magnetic reconnection in the upper atmosphere, which produced  $\text{H}\alpha$  ribbons.

In addition, the flare took place between two active regions. One possible explanation for the observations is that the new flux emergence triggered the reconnection between the two active regions. We do not mean that the new flux participated in the magnetic reconnection. The new flux may cause some instability, which triggered the reconnection of the existing current sheet above the filament. The reconnection may also play a role in starting the CME process; however, the triggering mechanism of the CME cannot be confirmed because of the data gap between the flare and CME data in current observations. It is also possible that the increase of the line-of-sight flux and of the transverse field are due to a flare-related change in the field line inclination in the flaring region (new asymmetric reconnected loops). More detailed modeling is beyond the scope of this paper.

We would like to thank the referee for the valuable comments. The work is supported by NSF under grants ATM 0313591, ATM 0233931, and AST 99-87366, NASA under grants NAG5-10910, NAG5-10212, and NAG5-12733, ONR under grant N00014-03-1-0093.

#### REFERENCES

- Amari, T., Luciani, J. F., Mikic, Z., & Linker, J. 2000, *ApJ*, 529, L49  
 Ambastha, A., Hagyard, M. J., & West, E. A. 1993, *Sol. Phys.*, 148, 277  
 Antiochos, S. K., DeVore, C. R., & Klimchuk, J. A. 1999, *ApJ*, 510, 485  
 Chen, J. 1989, *ApJ*, 338, 453  
 Chen, J., Wang, H., Zirin, H., & Ai, G. 1994, *Sol. Phys.*, 154, 261  
 Choe, G. S., & Cheng, C. Z. 2002, *Phys. Plasmas*, 9, 2330  
 Forbes, T. G. 2001, *Earth Planet Sci.*, 53, 423  
 Forbes, T. G., & Acton, L. W. 1996, *ApJ*, 459, 330  
 Forbes, T. G., & Lin, J. 2000, *J. Atmos. Sol.-Terr. Phys.*, 62, 1499  
 Forbes, T. G., & Priest, E. R. 1984, *Sol. Phys.*, 94, 315

- Forbes, T. G., & Priest, E. R. 1995, *ApJ*, 446, 377
- Green, L. M., Démoulin, P., Mandrini, C. H., & van Driel-Gesztelyi, L. 2003, *Sol. Phys.*, 215, 307
- Hagyard, M. J., Start, B. A., & Venkatakrishnan, P. 1999, *Sol. Phys.*, 184, 133
- Hagyard, M. J., Teuber, D., West, E. A., & Smith, J. B. 1984, *Sol. Phys.*, 91, 115
- Hagyard, M. J., Venkatakrishnan, P., & Smith, J. B., Jr. 1990, *ApJS*, 73, 159
- Handy, B. N., et al. 1999, *Sol. Phys.*, 187, 229
- Ji, H., Wang, H., Li, J., Jiang, Y., & Goode, P. R. 2004, *ApJ*, submitted
- Kosovichev, A. G., & Zharkova, V. V. 2001, *ApJ*, 550, L105
- Lin, R., et al. 2002, *Sol. Phys.*, 210, 3
- Low, B. C. 1994, *Plasma Phys.*, 1, 1684
- Low, B. C., & Zhang, M. 2002, *ApJ*, 564, L53
- Magara, T., Shibata, K., & Yokoyama, T. 1997, *ApJ*, 487, 437
- Mikic, Z., & Linker, J. A. 1994, *ApJ*, 430, 898
- Qiu, J., Lee, J., Gary, D. E., & Wang, H. 2002, *ApJ*, 565, 1335
- Qiu, J., Wang, H., Cheng, C. Z., & Gary, D. E. 2004, *ApJ*, 604, 900
- Scherrer, P. H., et al. 1995, *Sol. Phys.*, 162, 129
- Spirock, T. J., Yurchyshyn, V., & Wang, H. 2002, *ApJ*, 572, 1072
- Wang, H. 1992, *Sol. Phys.*, 140, 85
- Wang, H., Ewell, M. W., Zirin, H., & Ai, G. 1994, *ApJ*, 424, 436
- Wang, H., Ji, H., Schmahl, E. J., Qiu, J., Liu, C., & Na, D. 2002b, *ApJ*, 580, L177
- Wang, H., Spirock, T. J., Qiu, J., Ji, H., Yurchyshyn, V., Moon, Y., Denker, C., & Goode, P. R. 2002a, *ApJ*, 576, 497